

## Plasma Transmission Gratings for Compression of High-Intensity Laser Pulses

Matthew R. Edwards<sup>✉,†</sup> and Pierre Michel

*Lawrence Livermore National Laboratory, Livermore, California 94550, USA*



(Received 5 July 2021; revised 11 June 2022; accepted 16 June 2022; published 9 August 2022)

The peak power of a femtosecond laser is limited by the size and damage threshold of its solid-state optical components, with the final grating of a chirped pulse amplification compressor posing a challenging bottleneck on the path to higher-power systems. Practical hundred-petawatt to exawatt lasers will require optics that draw on the higher damage tolerance of plasma to manipulate high-intensity light, but plasma is a difficult medium to control and sets stringent limits on optical performance. Here we describe the design of a compact high-power laser system that uses plasma transmission gratings—with currently achievable parameters—for chirped pulse amplification. A double compression architecture compensates for the low angular dispersion of the plasma gratings. We explore the design constraints set by available plasma parameters and use particle-in-cell simulations to examine performance at high light intensity. These simulations suggest that the meter-scale final grating for a 10-PW laser could be replaced with a 1.5-mm-diameter plasma grating, allowing compression to, for example, 22 fs with 90% efficiency and providing a path towards compact multipetawatt laser systems.

DOI: 10.1103/PhysRevApplied.18.024026

### I. INTRODUCTION

Chirped pulse amplification (CPA) [1]—where a laser pulse is chromatically stretched, amplified, and compressed to avoid optics damage—revolutionized high-power laser design, with maximum peak power jumping from gigawatts to petawatts [2]. High-power lasers drive compact electron and ion accelerators [3,4], x-ray sources [5,6], and antimatter jets [7,8], but although these applications would benefit from higher available power, lasers today are bound by the size and damage thresholds of their optical components. A key constraint for contemporary systems is the delicate final CPA grating, which must withstand the full compressed power of the beam, resulting in meter-scale optics for 10-PW lasers [9]. The intensity limit of solid optics (approximately  $10^{12} \text{ W/cm}^2$ ) is not far below the ionization threshold of most materials, so advances in coatings can provide only marginal improvement: intensities above  $10^{13} \text{ W/cm}^2$  require plasma. Plasma optics has therefore become a vibrant research area, but despite promising

advances—including plasma mirrors [10–12], waveplates [13–15], and parametric plasma amplifiers based on stimulated Raman and Brillouin scattering [16–20]—there have been no viable demonstrations of efficient pulse compression at high power. For example, experimental studies of plasma amplifiers have underperformed theoretical predictions, in part due to the difficulty of creating a sufficiently uniform large plasma and the complexity of nonlinear plasma wave dynamics. The ideal path to higher-power lasers should therefore avoid both the intensity limit of solid-state optics and the recalcitrance of large-volume plasmas.

Volume transmission gratings are one-dimensional (1D) Bragg structures where the index of refraction ( $n$ ) is modulated [ $n = n_0 + \delta n(x)$ ] to diffract an incident beam. Different wavelengths of light diffract from transmission gratings at different angles, leading to chromatic angular dispersion. Although reflection gratings are the current standard for high-peak-power CPA lasers, transmission gratings have also been used for femtosecond pulse compressors [21], with experimental demonstrations of compression from 50 ps to 85 fs [22] and pulses as short as 13 fs [23]. A key advantage of transmission gratings as a candidate for reproduction in plasma is that the required modulation of the refractive index and the thickness are both relatively small, allowing small gas-density targets and reducing the impact of the nonlinearities and nonuniformity that plague Raman and Brillouin plasma amplifiers. A transmission grating design relying on angular dispersion and free-space propagation also requires less plasma

\*mredwards@stanford.edu

<sup>†</sup>Current address: Stanford University, Stanford, California, 94305, USA

Published by the American Physical Society under the terms of the [Creative Commons Attribution 4.0 International license](#). Further distribution of this work must maintain attribution to the author(s) and the published article's title, journal citation, and DOI.

and is less sensitive to inhomogeneity than a 1D grating compressor based on group delay via dispersive propagation within the grating itself [24,25]. The direct plasma analogue of reflective gratings—a variant of a plasma mirror where a grating structure is formed on an ionized solid surface [26–28]—faces both scientific and practical problems. Plasma expansion from the target makes forming a flat surface difficult, and a reflective plasma ( $N = n_e/n_c > 1$ , where  $n_e$  is the electron number density,  $n_c = \epsilon_0 m_e \omega^2/e^2$  is the plasma critical density for frequency  $\omega$ , and  $\epsilon_0$ ,  $e$ , and  $m_e$  are the vacuum permittivity and electron charge and mass) necessitates solid-density targets, with their attendant repetition-rate limits, debris issues, and experimental complexity. In comparison to solid-density reflective gratings, transmission gratings based on plasma formed from a gas would therefore be an attractive option for future high-repetition-rate high-peak-power (and thus high-average-power) lasers.

Here we propose a design for a laser pulse compressor based on a plasma volume transmission grating producing chromatic angular dispersion. This design offers a damage threshold several orders-of-magnitude higher than existing reflection gratings, needs only gas as the initial medium, is robust to variations in plasma conditions, and minimizes the plasma volume to make sufficient uniformity practical. By using achievable plasma parameters and avoiding solid-density plasma and solid-state optics, this approach offers a feasible path towards the next generation of high-power lasers.

## II. DESIGN

The typical high-power chirped-pulse-amplification laser consists of (1) a mode-locked oscillator producing a train of femtosecond pulses, (2) a stretcher that dispersively chirps each pulse to produce a longer pulse duration, (3) a sequence of amplifiers to increase pulse energy, and (4) a compressor that dramatically increases pulse power by dispersively recovering the femtosecond pulse duration [1], as shown in the left half of Fig. 1. In a standard system, the stretched pulse (whose duration might be between 200 ps and 2 ns) is fully compressed (to between 20 and 100 fs) after (4). The final grating in this compressor and any subsequent optics must be sized to accommodate the full peak power and is therefore large: at a damage threshold of  $2 \text{ TW/cm}^2$ , a 10-PW pulse requires optics more than 70 cm across. These postcompression optics are a bottleneck in reducing the optical size of a laser system and are the obvious place to use the high damage threshold of plasma. We can take an all-solid-state transmission grating compressor design [21–23] and replace the final grating with a plasma to dramatically increase the damage threshold of the overall system, drawn in Fig. 1 as the second compressor (5,6). However, since the angular dispersion

possible with a plasma grating is smaller than that achievable with solid-state reflection and transmission gratings, the distance  $b$  between the final two gratings becomes impractically large if the stretched pulse duration ( $\Delta\tau$ ) is long, as described more fully in Sec. II D. This precludes a single-stage plasma chirped pulse compression system. We avoid this issue using the dual-compressor architecture shown in Fig. 1, taking advantage of the fact that compressing from nanosecond to 10-ps duration requires most of the dispersion, but compressing from 10-ps to 10-fs duration has the largest impact on damage threshold. Broadly, optics are energy-flux limited for pulses longer than picoseconds (so pulse duration is less important) and intensity limited for femtosecond pulses. A combination of solid-state and plasma compression therefore allows both small optics and a small overall footprint.

Our proposed plasma-grating-based design partially compresses the pulse at step (4), resulting in a chirped pulse duration of 1–10 ps. This is shorter than the pulse in the amplifiers but two-to-three orders-of-magnitude longer (and thus lower peak power) than the femtosecond final pulse. The gratings and mirrors in this compressor and the beam transport line between it and the start of the second compressor (5) may therefore be smaller (in area) by this same two-to-three orders of magnitude. To achieve a final pulse duration of 20–100 fs, we pass the beam through a second compressor (5,6,7); in the simplest configuration this consists of three solid-state gratings and a final plasma grating (6). In Fig. 1 we have drawn the solid-state gratings as a pair of reflection gratings and a transmission grating, but any configuration of three grating passes that produces the correct angular and spatial chirp, along with the appropriate pulse front tilt, could work in this scheme. The second compressor reduces the 1–10 ps chirped duration to the 20–100 fs final desired pulse (7), where the only optic that sees the full final pulse intensity is the volume plasma transmission grating (6). As we will discuss in more detail, this design is constrained by the optical properties reasonably achievable with a plasma grating and by the desire to minimize both the size of the component optics and the overall footprint of the system.

This approach, which relies on the angular dispersion of a volume plasma transmission grating, offers several potential advantages over previous plasma-based proposals for generating high-peak-power pulses, including parametric plasma amplification, longitudinal compression in a plasma grating, and attosecond pulse generation by relativistic plasma mirrors. Plasma Raman [16,17,29,30] and Brillouin [18–20,31,32] amplifiers, based on the transfer of energy from a long-duration pump to a short high-power seed via electron or ion waves, respectively, have a long history of theoretical and computational studies, but have proven experimentally difficult in part because the required plasma volume is large and challenging to produce with sufficient uniformity. For example, if the

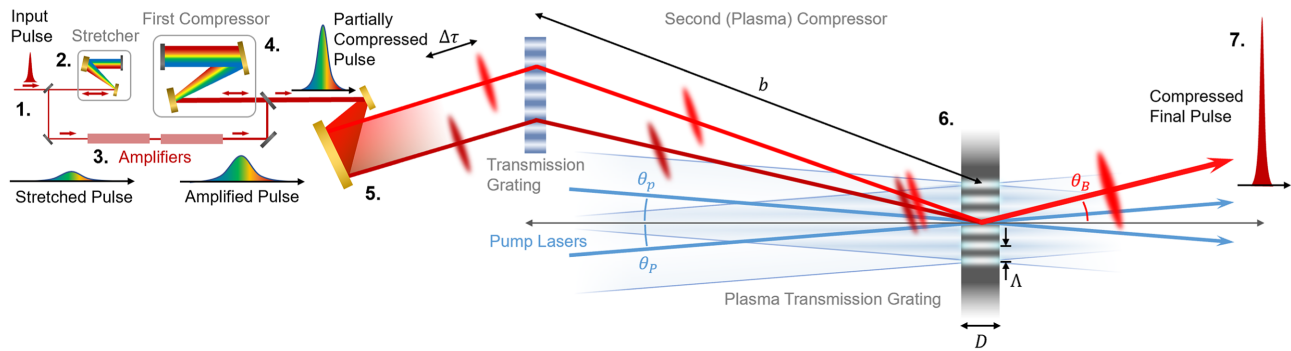


FIG. 1. Schematic of a plasma-grating-based laser system using a double-CPA architecture. The final grating is formed in a plasma by two short-pulse beams. An input femtosecond pulse from an oscillator is stretched, amplified, and compressed to 1–10 ps by the first stage (solid state) compressor. Compression from 1–10 ps to 10–50 fs occurs in the second stage, where only the plasma grating sees a pulse duration shorter than 1 ps and the concomitant high intensity.

plasma density changes throughout the interaction volume, the phase matching condition between the pump, the seed, and the plasma wave for Raman amplification cannot be met everywhere at once. Furthermore, the processes rely on Langmuir and ion-acoustic waves in regimes where nonlinearities and other parasitic instabilities may be important, sensitizing the system to plasma conditions. Compression by a relativistic plasma mirror could in principle produce a few-attosecond pulse from a few-femtosecond driver, dramatically increasing power [33,34], but the method is unsuitable for compressing a pulse that is not already few-cycle. Previous approaches to compression in plasma gratings [24,25] rely on the enhanced dispersion of a grating compared to a uniform plasma or using a chirped grating structure. In both cases the compression process will be sensitive to the plasma density, which is an issue because the density of laser-driven plasmas is difficult to control. The key advantage of using volume transmission gratings as angularly dispersive elements for compression is that, although it may still be difficult to produce a perfect plasma grating, imperfections in the plasma density will affect the diffraction efficiency (i.e., the energy of the diffracted pulse) but not its pointing or the final pulse duration. The compression is due to free-space propagation, and the angular dispersion of the grating depends only on the grating wavelength. Since this wavelength is set by the crossing angle and wavelength of the two pump beams—parameters that can be made very stable in experiment—we expect that this approach is capable of providing a degree of stability not accessible with other plasma compression mechanisms and may prove more feasible to build in practice.

The system through the first compressor is based on an established design that requires only slight modification to produce a partially compressed chirped pulse, so this manuscript focuses on the requirements that a plasma grating imposes on the second compressor, primarily on its final two gratings. In the following sections we discuss the

potential formation mechanisms of an appropriate plasma grating and the resultant relationships between grating size, bandwidth, and dispersion.

### A. Volume plasma transmission gratings

Consider two pump laser beams (wavelength  $\lambda_p$ ) crossed at a small angle ( $2\theta_p$ ) as illustrated in Fig. 1. Their interference will produce a 1D intensity modulation with wavelength  $\Lambda = \lambda_p/2 \sin \theta_p$ , which, in a medium with an intensity-dependent plasma response, will drive a 1D density modulation. Since the refractive index varies with the plasma density ( $n = \sqrt{1 - N}$ ), a density modulation directly produces an index modulation. Potential plasma mechanisms include (1) ponderomotive ion forcing [35–37], where ion-density modulations are driven by ponderomotive movement of plasma electrons; (2) spatially varying ionization (SVI) [38–40], where the highest-intensity regions of the interference pattern are above the ionization threshold, producing an alternating pattern of plasma and neutral gas; and (3) ponderomotive electron forcing, where electrons are ponderomotively driven, but the timescales are too short for significant ion motion [16,41]. A related nonplasma alternative (4) with lower intensity limits modulates neutral gas density to produce a nonionized optic [42]. Both the ponderomotive ion mechanism and spatially varying ionization support index modulations ( $\delta n$ ) of the order of 1% with picosecond persistence, which, although lower than those achievable with solid-state materials, is just sufficient to construct a useful diffractive optic for pulse compression.

Ion gratings created via the ponderomotive force have a well-developed theoretical basis [35,37,43,44] and have been demonstrated experimentally [45]. The interaction that results when two lasers cross with a frequency separation comparable to the ion wave frequency has been applied to cross-beam energy transfer [36,46], Brillouin plasma amplifiers, and plasma-based polarization optics

[15,47,48]. Here, we focus on the case where the two pump lasers are equal in intensity and frequency, and the resultant plasma density modulation is created via their interference with no reliance on a plasma wave, as described well, for example, by Lehmann and Spatschek [37]. The gratings are impulsively driven by the pump lasers, with the ion motion following on a picosecond timescale. Our system is different from the majority of studies on the formation of ion gratings in that the pump beams are near copropagating, but despite the resultant longer grating wavelength, the basic principles of grating formation still hold.

Ionization gratings—demonstrated in a series of experiments using femtosecond pump beams at the millijoule scale [38–40,49–51]—have a simpler theory, relying only on the static plasma density created by differing ionization rates in a standing intensity interference pattern. In fact, to effectively use an ionization grating, we want to avoid “plasma” effects altogether, with the probe beam arriving so soon after the pump beams that the grating has no time to hydrodynamically evolve. Experimental work has demonstrated plasma densities of up to  $2 \times 10^{19} \text{ W/cm}^2$  [39], diffraction efficiency of up to 18.7% [39], and grating lifetimes of tens to hundreds of picoseconds, limited by recombination and diffusion [40]. On the tens-of-femtoseconds timescale of a compressed pulse, these gratings can be treated as static. Experiments on ionization gratings have primarily been done in air or uniform-density gas environments, where the grating shape is set by the overlap volume of the two pump beams and is strictly neither a reflection nor a transmission grating; building the volume transmission gratings required for this compressor design requires a geometry restricted in the longitudinal direction, i.e., a gas jet or gas cell. A change in geometry should also help increase efficiency to the 50% or more required for a competitive compressor grating.

The plasma parameters achievable with these two mechanisms set the properties of the gratings we can use to design a compressor; their limited plasma density modulation amplitude means that we must carefully address the optical properties of the proposed grating.

## B. Grating size

The diffraction efficiency of volume transmission gratings depends on their extent in the direction of beam propagation, with the index modulation amplitude setting the optimal size. If a short-pulse laser with central wavelength  $\lambda_0$  and finite bandwidth  $\Delta\lambda$  [full width half maximum (FWHM)] strikes a transmission grating with large transverse size and sinusoidal index modulation [ $n = n_0 + n_1 \cos(2\pi x/\Lambda)$ ] at an incidence angle ( $\theta_0$ ) equal to the Bragg angle ( $\theta_B$ ) of the central wavelength [ $\theta_0 = \theta_B = \sin^{-1}(\lambda_0/2n_0\Lambda)$ ], the diffraction efficiency of

the component with wavelength  $\lambda$  is given by [52,53]

$$\eta = \sin^2(\kappa DB)/B^2, \quad (1)$$

where  $B = \sqrt{1 + (\Delta\alpha/2\kappa)^2}$ , the phase mismatch  $\Delta\alpha = -\pi(\lambda - \lambda_0)/(n_0\Lambda^2 \cos \theta_B)$ ,  $\kappa = \pi n_1/(\lambda \cos \theta_B)$ , and  $D$  is the grating thickness. For  $\lambda = \lambda_0$ , the phase mismatch is zero ( $B = 1$ ), and  $\eta = \sin^2 \kappa D$ . Note that in deriving this expression we have simplified a general periodic index modulation ( $\delta n$ ) to a sinusoidal one ( $n_1$ ); the effect of nonsinusoidal  $\delta n$  is considered in the section on nonideal gratings. Unlike for reflection gratings, where increasing thickness monotonically produces higher efficiency, transmission gratings must have a finite thickness to prevent energy returning to the zeroth-order beam. The condition  $\eta = 1$  sets, for minimum  $D$ ,  $\kappa D = \pi/2$  and, therefore,

$$D = \frac{\lambda_0 \cos \theta_B}{2n_1}. \quad (2)$$

For small  $\theta_B$ , this simplifies to  $D/\lambda_0 \approx 1/(2n_1)$ , so that, for  $2n_1 = 0.01$ , the grating must have  $D = 100\lambda_0$ .

## C. Grating bandwidth

Deviations of the laser wavelength or angle of incidence from the ideal Bragg angle will limit the diffraction efficiency, even if the grating thickness is ideal. Equation (1) can also be used to derive the wavelength ( $\Delta\lambda_g$ ) and angular ( $\Delta\theta_g$ ) bandwidths of a grating with thickness  $D = \pi/(2\kappa)$ , which are critical for determining the useful spectral range of the compressor and thus possible compressed pulse durations. For  $B \neq 1$ , Eq. (1) is transcendental, but for small bandwidth ( $\Delta\lambda_g/\lambda_0 \ll 1$ ) and neglecting the bulk shift in refractive index ( $n_0 \approx 1$ ), we can set  $\eta = 0.5$  to yield  $\Delta\alpha/(2\kappa) = C_\alpha \approx 0.8$  and the approximation for the FWHM bandwidth:

$$\frac{\Delta\lambda_g}{\lambda_0} \approx C_\alpha \frac{n_1}{2 \sin^2 \theta_B}. \quad (3)$$

The exact value of  $C_\alpha$  will vary depending on the metric for describing bandwidth and the desired efficiency but will generally be close to 1, and  $C_\alpha$  may safely be neglected for rough calculations. To efficiently diffract the incident laser pulse, we should satisfy  $\Delta\lambda < \Delta\lambda_g$ . From this expression, it is clear that it becomes difficult to meet the bandwidth requirement for a femtosecond laser pulse ( $\Delta\lambda/\lambda_0 \approx 0.1$ ) for angles greater than  $5^\circ$  if  $n_1$  is small (e.g.,  $n_1 < 10^{-3}$ ), which is why we focus on plasma mechanisms that can provide large  $n_1$ . Note that, given the previous constraints, this can also be thought of as resulting from the ratio of the grating thickness to wavelength, i.e.,  $\Delta\lambda_g/\lambda_0 \approx C_\alpha \Lambda/(2D \tan \theta_B)$ . For a transform-limited Gaussian pulse, the bandwidth condition also sets a minimum pulse duration  $\tau/T_L \approx \sin^2 \theta_B/n_1$ , where  $\tau$  is the

FWHM pulse duration and  $T_L$  is the laser optical period. For a  $\lambda_0 = 800$  nm pulse at  $\theta_B = 10^\circ$  and  $n_1 = 0.005$ , this gives a minimum pulse duration for moderately efficient compression of 8 fs.

Volume transmission gratings have a finite angular bandwidth; the efficiency drops if the probe is not incident at the Bragg angle. Although it is straightforward to construct a compressor where the probe is centered at the Bragg angle, the finite angular bandwidth also sets a more-difficult-to-avoid condition on the divergence, and thus  $f$ -number and minimum spot size. For a grating that has been tuned to have 100% efficiency at the Bragg angle ( $\kappa = \pi/2D$ ), we can use  $\Delta\alpha = 2\pi(\theta - \theta_0)/\Lambda$  [52] and the same condition on  $B$  as for the wavelength calculation to write

$$\Delta\theta_g \approx C_\alpha \frac{n_1}{\cos \theta_B \sin \theta_B} = C_\alpha \frac{\Lambda}{2D}. \quad (4)$$

The probe should meet  $\Delta\theta < \Delta\theta_g$ , so the probe  $f$  number ( $f \approx 1/\Delta\theta$ ) is limited by

$$f > \frac{1}{C_\alpha} \frac{\cos \theta_B \sin \theta_B}{n_1} = \frac{1}{C_\alpha} \frac{2D}{\Lambda}, \quad (5)$$

which, for a Gaussian pulse, gives a minimum spot size  $w_0/\lambda_0 > 4D/(C_\alpha \pi \Lambda) \approx D/\Lambda$ . For a high-efficiency grating, we should aim to exceed these inequalities by the greatest degree allowed by achievable dispersion, i.e.,  $\Delta\lambda/\lambda_0 \ll \Lambda/(D \tan \theta_B)$ ,  $\Delta\theta \ll \Lambda/D$ ,  $w_0/\lambda_0 \gg D/\Lambda$ .

## D. Dispersion

The angular dispersion produced by these plasma transmission gratings is critical for their use in a chirped pulse amplification system. As shown by Fig. 1, in a grating pair (separated by distance  $b$ ) the angular dispersion of the gratings creates a chromatic path length difference ( $\Delta b$ ); the second grating cancels the angular dispersion of the first, leaving only spatial and temporal chirp. The path length difference produces a chromatic time delay  $\Delta\tau = \Delta b/c$  that can be used to compress a chirped pulse with maximum duration of approximately  $\Delta\tau$ .

The grating equation ( $\lambda/\Lambda = \sin \theta_0 + \sin \theta$ ) gives the first-order diffraction angle of wavelength  $\lambda$ ,  $\theta = \sin^{-1}(\lambda/\Lambda - \sin \theta_0)$ , quantifying the angular dispersion induced in a finite-spectrum pulse by a transmission grating. In a configuration like that illustrated in Fig. 1, the transit time difference ( $\Delta\tau$ ) between colors separated by  $\Delta\lambda$  is given by [21]

$$\frac{\Delta\tau}{\Delta\lambda} = \frac{b\lambda}{c\Lambda^2} \left[ \frac{1}{1 - (\lambda/\Lambda - \sin \theta_B)^2} \right], \quad (6)$$

where  $c$  is the speed of light. Simplifying for  $\Delta\lambda/\lambda_0 \ll 1$ , this can be written in the more useful form

$$\frac{b_{[\text{mm}]}}{\Delta\tau_{[\text{ps}]}} \approx \frac{0.075}{\tan^2 \theta_B} \left( \frac{\Delta\lambda}{\lambda_0} \right)^{-1}. \quad (7)$$

This equation gives the distance between the two gratings ( $b_{[\text{mm}]}$ ) required per picosecond of stretched pulse duration ( $\Delta\tau_{[\text{ps}]}$ ) to compress a chirped pulse to its transform limit. For example, a 10-ps chirped pulse with  $\Delta\lambda/\lambda_0 = 0.1$  incident at  $\theta_0 = \theta_B = 10^\circ$  would require a distance  $b = 240$  mm between the final two gratings of its compressor. If the Bragg angle is only  $\theta_B = 1^\circ$ , the required spacing becomes almost 25 m. Unlike the conditions on bandwidth, which encourage smaller  $\theta_B$  (and thus larger  $\Lambda$ ), the constraint on maximum  $b$  encourages as large a  $\theta_B$  as possible. With limited  $n_1$ , the central issue for the design of a compressor based on plasma gratings is ensuring that the overall size is compact enough to be practical while the spectral and angular bandwidths are sufficiently large to efficiently manipulate the desired probe.

Figure 2 shows the design space set by the tension between these two factors. Using Eq. (7), the required grating-separation-to-stretched-pulse-duration ratio ( $b/\Delta\tau$ ) is plotted as a function of  $\theta_B$  and  $\Delta\lambda/\lambda_0$ . For a specified pulse bandwidth and stretched pulse duration, the distance between the two gratings decreases for increased  $\theta_B$ ; a compact design encourages large  $\theta_B$ . However, the available  $n_1$  sets a limit on the bandwidth of the plasma grating via Eq. (3). The red lines mark the maximum Bragg angle that can be used for a specific  $n_1$  as a function of  $\Delta\lambda/\lambda_0$ . High-efficiency diffraction requires staying well below these lines. For example, with  $\Delta\lambda/\lambda_0 = 0.1$  and  $n_1 = 0.005$ , we are restricted to  $\theta_B < 10^\circ$ , corresponding to  $b_{[\text{mm}]}/\Delta\tau_{[\text{ps}]} > 30$ .

In fact, with  $n_1 = 0.005$ , we are limited to  $b_{[\text{mm}]}/\Delta\tau_{[\text{ps}]} > 30$  for most femtosecond-pulse bandwidths. Since standard CPA lasers have stretched pulse durations of the order of 1 ns, this puts single-stage chirped pulse amplification outside the reach of currently practical plasma transmission gratings; for  $\Delta\tau = 1$  ns and  $b/\Delta\tau = 30$  mm/ns, we would need  $b = 30$  m. However, we can mitigate this issue by using—as drawn in Fig. 1—a double CPA architecture, where solid-state gratings reduce the pulse duration from 1 ns to 10 ps and a second compressor with a plasma-based final optic provides compression from 10 ps to 10 fs. In this case, the final compressor grating separation is only 30 cm, and the solid-state gratings must tolerate powers 3 orders-of-magnitude lower than the final plasma optic, allowing every solid-state component in the laser to be made substantially smaller.

To compress 1–10 ps stretched pulses without prohibitive path lengths,  $b_{[\text{mm}]}/\Delta\tau_{[\text{ps}]}$  should fall between 10 and about 300, which requires  $n_1 > 10^{-3}$ . Both controlled ionization and ponderomotive ion gratings can satisfy this

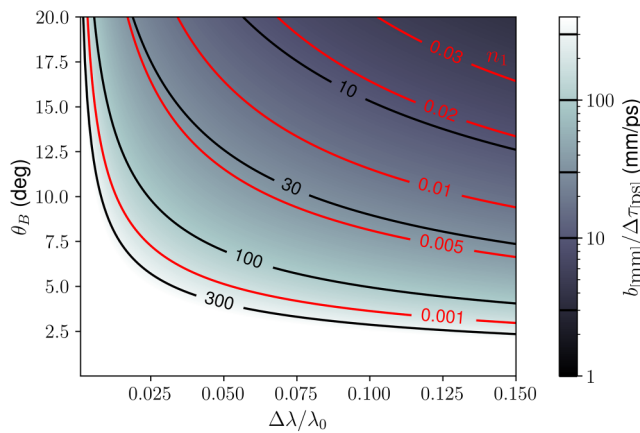


FIG. 2. Design space of a plasma-transmission-grating-based compressor, showing the required distance between gratings ( $b$ ) for the pulse bandwidth ( $\Delta\lambda/\lambda_0$ ) and grating Bragg angle ( $\theta_B$ ). The color scale indicates the distance  $b$  required for every picosecond of stretched pulse duration ( $\Delta\tau$ ), and the red lines indicate the upper bound of the design envelope for an available value of  $n_1$ .

condition, providing an envelope in  $\Delta\lambda$ - $\theta_B$  space between the  $n_1$  and  $b/\Delta\tau$  curves where construction of a compact high-power laser system based on plasma transmission gratings is feasible.

### III. RESULTS

Uniform transmission gratings are analytically tractable, but the propagation of light through a diffractive element with arbitrary geometry must be attacked numerically. Here we use both a paraxial propagation solver and particle-in-cell (PIC) simulations to show that the above theory predicts the performance of plasma gratings and to explore achievable pulse compression, nonideal grating properties, and nonlinear propagation effects.

#### A. Pulse compression

This approach to pulse compression requires the removal of the probe's angular chirp as it passes through the final grating. To simulate the probe propagation, we spectrally solve the paraxial wave equation

$$(2ik_0\partial_z + \nabla_{\perp}^2) E(\mathbf{r}) = -2k_0^2 E(\mathbf{r}) \frac{\delta n(\mathbf{r})}{n_0}, \quad (8)$$

where the electric field of the light wave ( $\tilde{E}$ ) is decomposed into envelope and high-frequency components as  $\tilde{E}(\mathbf{r}, t) = \frac{1}{2}E(\mathbf{r}) \exp[i(k_0 z - \omega_0 t)] + \text{c.c.}$ , with  $k_0$  the wave number,  $\omega_0$  the frequency, and  $\mathbf{r}$  the vector position. The refractive index is separated into uniform and nonuniform components,  $n(\mathbf{r}) = n_0 + \delta n(\mathbf{r})$ , such that  $n^2(\mathbf{r}) \approx n_0^2 + 2n_0\delta n(\mathbf{r})$ , with  $k_0 = n_0\omega_0/c$ . The calculations are performed in two steps. (1) First we calculate the paraxial

propagation of the two pumps assuming no self-action with the nonlinear medium [i.e., no right-hand-side term in Eq. (8)], creating a map of the pump interference intensity across all space,  $I(\mathbf{r})$ . Relating pump intensity to refractive index change by an arbitrary function  $f$ —chosen based on the targeted plasma mechanism—we produce a map of the refractive index in space,  $\delta n(\mathbf{r}) = f(I(\mathbf{r}))$ . In this paper we generally assume a quadratic nonlinearity [e.g.,  $f(I) = n_2 I$ ]. (2) In the second part of the calculation, the probe is propagated through the refractive index map derived in the first, with finite steps inside the nonlinear medium. Although this method does not allow for simulation of nonlinear time-dependent effects (for which we use PIC), it provides a powerful and efficient method for evaluating the propagation and dispersion of pulses over long distances.

Figures 3(a) and 3(b) show the 3D propagation of a single-frequency (infinite-duration)  $\lambda_0 = 800$  nm probe ( $\theta_0 = 10^\circ$ ) from left to right through a transmission grating formed by the interference of two pumps that drive an intensity-dependent index modulation ( $n_1 = 0.00525$ ) in a finite medium ( $D = 80 \mu\text{m}$ ). Here, 99.7% of the incident probe energy deflects into the first order. Figure 3(b) shows that the diffracted beam maintains the spatial quality of the incident probe; an ideally formed transmission grating allows almost perfect manipulation of light. The beam waists of the pumps are  $200 \mu\text{m}$  and that of the probe is  $150 \mu\text{m}$ . The simulations use 8192 points in both transverse dimensions and both real and frequency space, with 20 longitudinal ( $z$ ) positions evaluated inside the plasma.

If we change the wavelength of the incident light while keeping the same incidence angle [Fig. 3(c)], the efficiency of the grating drops and the first-order diffraction angle ( $\theta_1$ ) changes. Both the observed efficiency ( $\eta$ ) and the diffraction angle closely follow analytic predictions [Eq. (1) and the grating equation, respectively], with this grating providing greater than 80% efficiency across a 60-nm bandwidth. Since the propagation of light is time-reversal symmetric, this problem is symmetric over  $z = 0$ , and we can expect that light with wavelength  $\lambda$  incident at varied angle  $\theta_1(\lambda)$  will be diffracted to  $\theta_0 = \theta_B$ . We can therefore construct an angularly, spatially, and temporally chirped pulse—as would be produced by the penultimate grating in a compressor—with the chirp chosen such that after propagation over a specified distance of free space a point is reached ( $z = 0$ ) where the spatial and temporal chirps are instantaneously zero. An alternative view is to divide a pulse into frequency components: although each frequency component of the pulse propagates at a different angle, there is a point in space where they are exactly coincident in space with zero relative phase. A transmission grating placed at this point undoes the angular chirp (diffracts each frequency component in the same direction) and the resulting unchirped pulse will propagate away from the grating without distortion.

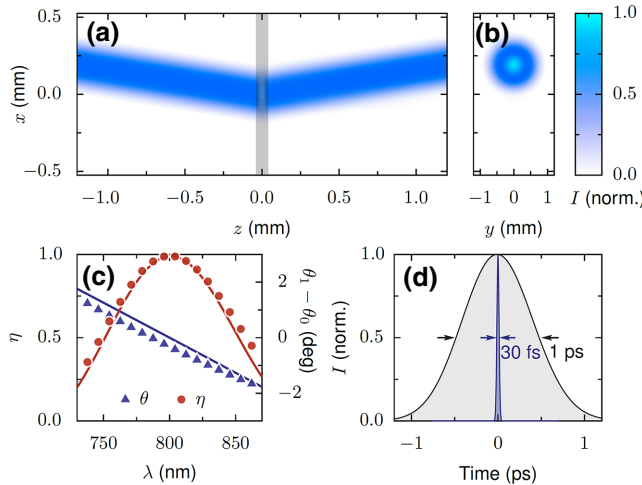


FIG. 3. Paraxial propagation calculations of light travelling through a plasma grating. (a) An 800-nm probe (blue) propagates from left to right through a plasma grating formed by two pumps in a thin ( $D = 80 \mu\text{m}$ ) gas sheet (gray region). The colormap shows normalized intensity. (b) Transverse profile of the diffracted beam. (c) Variation of efficiency and first-order diffraction angle with probe wavelength, showing that numerically calculated solutions closely follow the analytic theory (lines). (d) Initial and compressed pulse durations of a pulse after propagation through 100 mm of free space and the plasma grating.

To simulate this, the probe is divided into  $N_\omega$  appropriately weighted frequency components whose evolutions are evaluated separately. The propagated pulse is then found by adding these frequency components together, accounting for both phase and amplitude. In Fig. 3(d), conducted in two dimensions, the probe is divided into 128 separate frequency components with different initial positions and incident angles. The plasma properties are the same as in the other parts of Fig. 3. Figure 3(d) shows the time envelope of such a pulse 100 mm before (duration 1 ps) and 5 mm after (duration 30 fs) the same grating shown in Fig. 3(a). The grating has diffracted all frequency components of the incident pulse with high efficiency and entirely undone the angular chirp, providing a high-quality 30-fs pulse that propagates through free space without further distortion. Similar performance is observed in simulations of an entire sequence of four gratings, which, with appropriately chosen spacing, can compress a temporally chirped (but spatially and angularly uniform) initial pulse, although the most straightforward laser system designs would use plasma only for the final transmission optic.

### B. Nonideal grating profiles

High efficiency can also be achieved with more complex grating profiles and modulation shapes. This is particularly important because a gas target will not produce a

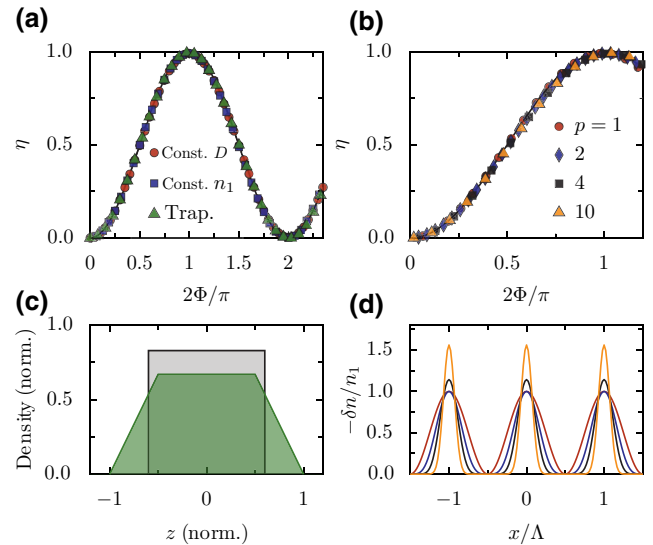


FIG. 4. Paraxial propagation solver calculations of grating efficiency in the presence of deviations from the ideal grating shape. (a) First-order diffraction efficiency ( $\eta$ ) as a function of grating strength for (1) rectangular grating profiles with constant  $D = 100\lambda_0$  and varied  $n_1$  (red circles); (2) rectangular profiles with constant  $n_1 = 0.005$  and varied  $D$  (blue squares); and (3) trapezoidal profiles with varied  $n_1$  (green triangles), as illustrated in (c). (b) Grating efficiency for the varied functional form of the pump intensity to index modulation map:  $\delta n \propto I^p$  with  $\Phi$  calculated based on the component  $n_1$ . (c) Rectangular and trapezoidal grating profiles. (d) Transverse index modulations of different orders, corresponding to data in (b).

rectangular density profile with step-function edges; density will decrease smoothly to zero. The plasma may also not respond linearly to the pumps. The ionization mechanism, for example, produces an index modulation that is a highly nonlinear function of the pump intensity. As we show here, neither of these issues prevents the construction of an efficient grating.

By the grating integral method [52], as long as the  $z$  profile varies slowly compared to the probe wavelength, we can generalize the expression for grating strength  $\Phi = \kappa D$  as

$$\Phi = \int_{-\infty}^{\infty} \kappa(z) dz, \quad (9)$$

where  $\kappa(z)$  is evaluated for each location in  $z$ . As Fig. 4 shows, when the grating is simulated with a paraxial code, the diffraction efficiency closely follows Eq. (1) over a wide range of density modulation amplitudes and grating thicknesses for both rectangular and trapezoidal density profiles [illustrated in Fig. 4(c)]. The maximum efficiency ( $\eta \approx 1$ ) is reached when  $\Phi = \pi/2$  for both profile shapes, indicating that, as long as  $\Phi$  can be controlled (e.g., by changing the gas density), variations of the profile shape may be neglected. The simulations presented in

Fig. 4 are conducted in two dimensions, with  $\lambda_p = 800$  nm,  $\theta_p = 10^\circ$ , 500- $\mu\text{m}$  pump beam waists,  $\lambda_0 = 800$  nm,  $\theta_0 = 10^\circ$ , and a 100- $\mu\text{m}$  probe beam waist. The simulations use 8192 transverse points in both real and frequency space, with 81  $z$ -direction steps within the plasma volume.

We have thus far assumed that the plasma modulation is perfectly sinusoidal, i.e.,  $\delta n = n_1 \cos(2\pi x/\Lambda)$ , but in general  $\delta n$  may have arbitrary functional form. However, any  $\delta n$  which is periodic in  $x$  with wavelength  $\Lambda$  may be expressed as a sum of harmonics with coefficients  $n_m$  and wavelengths  $\Lambda/m$ , noting that the Bragg angles of the component gratings will be  $m\theta_B$ . The total diffraction of an arbitrary grating can be found by treating each sinusoidal frequency component of that grating separately; since we are in the Bragg, rather than Raman-Nath, regime, a beam incident at  $\theta_B$  for the first-order sinusoidal grating will be well outside the angular bandwidth of the higher-order gratings:  $\Delta\theta \ll \theta_B$ . The higher-order components may therefore be neglected in our analysis, and complete diffraction to the first order is possible, provided we use  $n_1$  rather than the total  $\delta n$  to assess the grating strength. This is shown in Fig. 4(b), where efficiency closely follows Eq. (1) for  $\delta n \propto I^p$  for a range of values of  $p$ . In Fig. 4(d), these different values of  $p$  produce different grating shapes and ratios of  $\delta n$  to  $n_1$ . Significantly, there is no requirement that our plasma mechanism produce a density modulation that linearly depends on pump intensity; arbitrary functional forms are usable.

### C. Intensity limits

Like conventional optics, plasma optics have intensity or energy flux thresholds above which performance suffers. The paraxial solver does not capture the dynamics of the laser-plasma interaction, including the nonlinear effects that will limit performance at high intensity. Instead, we use the PIC code EPOCH [54] to simulate the high-intensity performance of an ion-ponderomotive grating as an example plasma-based final-stage optic.

Figure 5 shows results from 2D PIC simulations of pulse compression via a plasma grating. Two 600-fs pumps ( $\lambda_p = 1 \mu\text{m}$ ,  $I = 2 \times 10^{15} \text{ W/cm}^2$ ) are crossed ( $\theta_p = 11.5^\circ$ ) in a fully ionized hydrogen plasma with a trapezoidal profile and peak density  $n_e = 8.7 \times 10^{19}$ . Ponderomotively driven electrons drag the ions away from regions of high intensity, forming a plasma grating structure in picoseconds, as shown in grayscale in Fig. 5(d). The simulation covers an area of  $120 \times 120 \mu\text{m}^2$  with resolution  $\Delta x = \Delta z = 26.7 \text{ nm}$  ( $\lambda_0/\Delta x = 30$ , 4500  $\times$  4500 cells). For the plasma, we use electron and ion temperatures  $T_e = 10 \text{ eV}$  and  $T_i = 1 \text{ eV}$ , respectively, and 20 macroparticles per cell. The simulation approximated an infinite width plasma with periodic boundary conditions in the transverse ( $x$ ) direction.

An angularly, spatially, and temporally chirped probe—as would be produced by the penultimate grating—is constructed from 500 separate frequency components selected with appropriate weighting from a bandwidth (with central wavelength  $\lambda_0 = 800$  nm) corresponding to a 22-fs unchirped pulse and added together at the boundary with central angle  $\theta_0 = 9.2^\circ$ . The angular chirp is chosen so that each frequency component is diffracted to the same angle by the grating, and the spatial and temporal chirps are chosen so that propagation to  $z = 0$  through free space reduces both to zero. Pulse front tilt is also introduced so that the diffracted pulse has a flat front. At  $z = -100 \text{ mm}$ , this probe has a duration of 1 ps, a sixth-order super-Gaussian transverse profile with 75  $\mu\text{m}$  full width half maximum, and is delayed 2 ps with respect to the pumps. Figures 5(a)–5(c) show how the phase fronts of the probe bream shift as it propagates through the grating; in Fig. 5(a), the phase fronts correspond to propagation at  $\theta = -9.2^\circ$ , in Fig. 5(b), interference between the almost-equal-energy diffracted and undiffracted components create an intensity modulation in  $x$ , and in Fig. 5(c), with most of the energy diffracted into the first order, the phase fronts correspond to propagation at  $\theta = +9.2^\circ$ , with some modulation due to interference with the residual zeroth-order beam.

After passage through the grating, the probe is followed with a moving window for several millimeters of propagation to ensure that the angular chirp has been adequately removed from the diffracted pulse. The intensity envelopes of the diffracted and residual zeroth-order probe are shown in Figs. 5(e) and 5(f), respectively. The diffraction efficiency into the first order is 88%. The high-intensity diffracted probe maintains good spatial quality and a 22-fs pulse duration [Fig. 5(g)] as it propagates in free space after the grating interaction. The probe intensity ( $3 \times 10^{17} \text{ W/cm}^2$ ), diameter (75  $\mu\text{m}$ ), and compressed duration (22 fs) correspond to a 13-TW laser with 300 mJ of energy; we have replaced the several-centimeter-scale final grating for a 10-TW laser with one less than 100  $\mu\text{m}$  across.

Nonlinearities at high probe intensity cause diffraction efficiency to fall, as shown for a 30-fs probe above  $5 \times 10^{17} \text{ W/cm}^2$  in Fig. 5(h). These simulations have reduced transverse size (10  $\mu\text{m}$ ) and spatial resolution ( $\Delta x = \Delta z = 32 \text{ nm}$ ,  $\lambda_0/\Delta x = 25$ ), with an infinite-transverse-width seed (periodic boundary conditions), so there is no drop in efficiency associated with the finite  $f$  number of the probe as there is for the simulation shown in Figs. 5(a)–5(g). The peak pulse intensity is changed in eight separate simulations between  $10^{17}$  and  $5 \times 10^{18} \text{ W/cm}^2$ . Additional simulations below  $10^{17} \text{ W/cm}^2$  showed no significant dependence of efficiency on intensity. The diffraction efficiency remains above 95% for intensities up to  $7 \times 10^{17} \text{ W/cm}^2$ , almost the relativistic threshold. Above this intensity, the probe laser is sufficiently strong to disrupt the plasma grating within 30 fs,

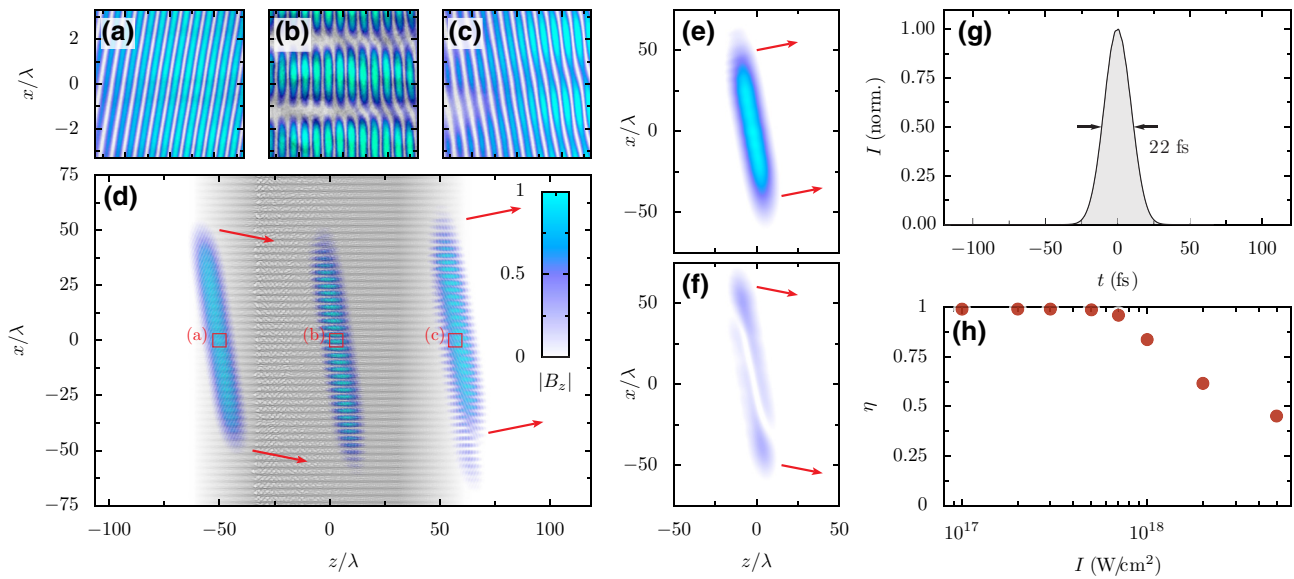


FIG. 5. PIC simulations of a probe laser crossing a plasma volume transmission grating. (a)–(d) The magnetic field amplitude (blue) and plasma density (gray) of a probe laser crossing an ion-ponderomotive grating formed by two pump lasers in a fully ionized hydrogen plasma, with (d) the probe shown at three different times. The red boxes mark the locations of the enlarged images of the probe phase fronts (a) before, (b) during, and (c) after the propagation of the probe through the grating. (f),(e) The intensity envelopes of the separated (e) diffracted and (f) zeroth-order probes after the grating. (h) The intensity envelope in time of the diffracted probe. (g) Diffraction efficiency for an infinitely wide 30-fs probe as a function of intensity.

leading to a distorted beam profile and a lower diffraction efficiency.

#### IV. DISCUSSION

The ability to manipulate light with plasma is critical for the development of higher-power lasers, since no other material can tolerate the required intensity and energy fluxes. Plasma gratings, specifically, allow compression of pulses to high peak power, providing a crucial step in the production of ultra-high-intensity light fields.

The practical application of plasma optics requires that the probe laser manipulated by the grating be more intense or of higher energy than the pump lasers that were used to create the grating. In the ponderomotive ion grating case illustrated in Fig. 5, the peak probe intensity at which efficient diffraction is possible ( $7 \times 10^{17} \text{ W/cm}^2$ ) is a factor of 350 higher than the pump intensity, corresponding to a probe that has 9 times more energy flux than both the pumps combined. Since the area of the pumps on the grating is similar to the area of the probe, the intensity and energy flux ratios can be directly translated to peak power and energy; the power required by the pumps is < 1% that of the probe, and including pump energy drops the total compressor energy efficiency by about 10%. Experimental work on spatially varying ionization gratings [39,55] suggests that the mechanism also supports the manipulation of probes with higher intensities than the pumps.

Although plasmas are extremely damage resistant, every plasma mechanism has a maximum tolerable intensity and energy flux before diffraction efficiency drops or the probe pulse becomes distorted. For SVI gratings, this limit is set by probe-driven ionization. For ponderomotive ion gratings, the relativistic plasma response causes probe distortion and changes the effective index modulation, setting an upper limit on the intensity. For both mechanisms, filamentation may be an issue for gratings that are too long. However, even with these limits, plasma gratings can operate at intensities almost 6 orders-of-magnitude higher than solid-state conventional gratings.

Based on the results presented in this paper, we can approximate the size of a plasma-transmission-grating-based petawatt-class laser. Consider a system designed to produce 20-fs 1-PW (20 J) pulses at 800 nm. Using approximate energy flux and peak intensity limits of  $4 \text{ J/cm}^2$  and  $2 \times 10^{12} \text{ W/cm}^2$ , respectively, for solid optics [56], a pulse compressed to 10 ps in the first compressor would require a beam diameter of less than 3 cm for all but the final optic of the second compressor. The final (plasma) optic, operating at an intensity of  $5 \times 10^{17} \text{ W/cm}^2$  need only be 0.5 mm in diameter to produce a 20-fs output pulse. At the conditions shown in Fig. 5, the pump lasers required for a 0.5-mm diameter plasma grating ( $I_p = 2 \times 10^{15} \text{ W/cm}^2$ ) would each have to provide 5 TW for 600 fs (3 J). Suitable targets to form the plasma grating might include gas, shock [57,58] or cluster [59] jets, gas cells [60], or, dropping the advantages of gas targets, nanofoil

or thin liquid films [61], which, given time to hydrodynamically expand after ionization, would be suitable for ponderomotive gratings.

With its largest optics at the centimeter scale, a plasma-based design for a 1-PW laser is only as large as a contemporary 10-TW laser. Scaling up, 10-PW (10-cm solid gratings, 1.5-mm plasma grating) and 100-PW lasers (30-cm solid gratings, 5-mm plasma grating) need only be as large as current 100-TW and 1-PW lasers, respectively. A practical design might require the final stage compression to be done immediately before the experimental target; in this case, all transport mirrors could be sized for the 10-ps-stretched pulse duration, allowing substantially more compact experimental facilities. Plasma optics can also focus high-intensity beams [62–65], allowing an entirely plasma-based final stage for high-power high-intensity laser facilities.

In summary, we have outlined the design of a plasma-based chirped-pulse-amplification laser based on angular dispersion from plasma transmission gratings and have used a particle-in-cell code to simulate the formation and performance of such a system. Any medium that can support an optical-quality index modulation of at least order  $10^{-3}$  should be suitable for a design in this parameter space, but we have highlighted spatially variant ionization and ponderomotively driven ion structures as plasma mechanisms that are robust to high laser intensity and energy flux and for which sufficiently high-index modulations have been demonstrated. The use of plasma transmission gratings as an approach to laser pulse compression imposes minimal requirements for plasma uniformity and quality, offering a path to compact high-power light sources feasible with current technology.

## ACKNOWLEDGMENTS

This work was performed under the auspices of the U.S. Department of Energy by Lawrence Livermore National Laboratory under Contract DE-AC52-07NA27344. Support was provided by the LLNL-LDRD Program under Projects No. 20-ERD-057 and No. 21-LW-013.

- [1] D. Strickland and G. Mourou, Compression of amplified chirped optical pulses, *Opt. Commun.* **55**, 447 (1985).
- [2] C. Danson, D. Hillier, N. Hopps, and D. Neely, Petawatt class lasers worldwide, *High Power Laser Sci. Eng.* **3**, e3 (2015).
- [3] C. Geddes, C. Toth, J. Van Tilborg, E. Esarey, C. Schroeder, D. Bruhwiler, C. Nieter, J. Cary, and W. Leemans, High-quality electron beams from a laser wakefield accelerator using plasma-channel guiding, *Nature* **431**, 538 (2004).
- [4] A. Macchi, M. Borghesi, and M. Passoni, Ion acceleration by superintense laser-plasma interaction, *Rev. Mod. Phys.* **85**, 751 (2013).

- [5] F. Albert and A. G. Thomas, Applications of laser wakefield accelerator-based light sources, *Plasma Phys. Controlled Fusion* **58**, 103001 (2016).
- [6] M. R. Edwards and J. M. Mikhailova, The x-ray emission effectiveness of plasma mirrors: Reexamining power-law scaling for relativistic high-order harmonic generation, *Sci. Rep.* **10**, 5154 (2020).
- [7] H. Chen, F. Fiuzza, A. Link, A. Hazi, M. Hill, D. Hoarty, S. James, S. Kerr, D. Meyerhofer, J. Myatt, *et al.*, Scaling the Yield of Laser-Driven Electron-Positron Jets to Laboratory Astrophysical Applications, *Phys. Rev. Lett.* **114**, 215001 (2015).
- [8] G. Sarri, K. Poder, J. Cole, W. Schumaker, A. Di Piazza, B. Reville, T. Dzelzainis, D. Doria, L. Gizzii, G. Grittani, *et al.*, Generation of neutral and high-density electron-positron pair plasmas in the laboratory, *Nat. Commun.* **6**, 6747 (2015).
- [9] F. Lureau, O. Chalus, G. Matras, S. Laux, C. Radier, O. Casagrande, C. Derycke, S. Ricaud, G. Rey, T. Morbieu, *et al.*, in *Solid State Lasers XXIX: Technology and Devices*, Vol. 11259 (International Society for Optics and Photonics, San Fransisco, California, 2020), p. 112591J.
- [10] C. Thaury, F. Quéré, J.-P. Geindre, A. Levy, T. Cecotti, P. Monot, M. Bougeard, F. Réau, P. d’Oliveira, P. Audebert, R. Marjoribanks, and Ph. Martin, Plasma mirrors for ultrahigh-intensity optics, *Nat. Phys.* **3**, 424 (2007).
- [11] J. M. Mikhailova, A. Buck, A. Borot, K. Schmid, C. Sears, G. D. Tsakiris, F. Krausz, and L. Veisz, Ultra-high-contrast few-cycle pulses for multipetawatt-class laser technology, *Opt. Lett.* **36**, 3145 (2011).
- [12] M. R. Edwards, N. M. Fasano, T. Bennett, A. Griffith, N. Turley, B. M. O’Brien, and J. M. Mikhailova, A multi-terawatt two-color beam for high-power field-controlled nonlinear optics, *Opt. Lett.* **45**, 6542 (2020).
- [13] P. Michel, L. Divol, D. Turnbull, and J. Moody, Dynamic Control of the Polarization of Intense Laser Beams via Optical Wave Mixing in Plasmas, *Phys. Rev. Lett.* **113**, 205001 (2014).
- [14] K. Qu, Q. Jia, and N. J. Fisch, Plasma  $q$ -plate for generation and manipulation of intense optical vortices, *Phys. Rev. E* **96**, 053207 (2017).
- [15] D. Turnbull, C. Goyon, G. Kemp, B. Pollock, D. Mariscal, L. Divol, J. Ross, S. Patankar, J. Moody, and P. Michel, Refractive Index Seen by a Probe Beam Interacting with a Laser-Plasma System, *Phys. Rev. Lett.* **118**, 015001 (2017).
- [16] V. M. Malkin, G. Shvets, and N. J. Fisch, Fast Compression of Laser Beams to Highly Overcritical Powers, *Phys. Rev. Lett.* **82**, 4448 (1999).
- [17] Y. Ping, W. Cheng, S. Suckewer, D. S. Clark, and N. J. Fisch, Amplification of Ultrashort Laser Pulses by a Resonant Raman Scheme in a Gas-Jet Plasma, *Phys. Rev. Lett.* **92**, 175007 (2004).
- [18] A. Andreev, C. Riconda, V. Tikhonchuk, and S. Weber, Short light pulse amplification and compression by stimulated Brillouin scattering in plasmas in the strong coupling regime, *Phys. Plasmas* **13**, 053110 (2006).
- [19] M. R. Edwards, Q. Jia, J. M. Mikhailova, and N. J. Fisch, Short-pulse amplification by strongly-coupled stimulated Brillouin scattering, *Phys. Plasmas* **23**, 083122 (2016).

- [20] J.-R. Marquès, L. Lancia, T. Gangolf, M. Blecher, S. Bolaños, J. Fuchs, O. Willi, F. Amiranoff, R. Berger, M. Chiaramello, *et al.*, Joule-Level High-Efficiency Energy Transfer to Subpicosecond Laser Pulses by a Plasma-Based Amplifier, *Phys. Rev. X* **9**, 021008 (2019).
- [21] T.-Y. Yang, P.-P. Ho, A. Katz, R. Alfano, and R. A. Ferrante, Femtosecond laser pulse compression using volume phase transmission holograms, *Appl. Opt.* **24**, 2021 (1985).
- [22] J.-K. Rhee, T. S. Sosnowski, T. B. Norris, J. A. Arns, and W. S. Colburn, Chirped-pulse amplification of 85-fs pulses at 250 kHz with third-order dispersion compensation by use of holographic transmission gratings, *Opt. Lett.* **19**, 1550 (1994).
- [23] A. Villamarín, I. Sola, M. Collados, J. Atencia, O. Varela, B. Alonso, C. Méndez, J. San Román, I. Arias, L. Roso, *et al.*, Compensation of second-order dispersion in femtosecond pulses after filamentation using volume holographic transmission gratings recorded in dichromated gelatin, *Appl. Phys. B* **106**, 135 (2012).
- [24] H.-C. Wu, Z.-M. Sheng, and J. Zhang, Chirped pulse compression in nonuniform plasma Bragg gratings, *Appl. Phys. Lett.* **87**, 201502 (2005).
- [25] H.-C. Wu, Z.-M. Sheng, Q.-J. Zhang, Y. Cang, and J. Zhang, Manipulating ultrashort intense laser pulses by plasma Bragg gratings, *Phys. Plasmas* **12**, 113103 (2005).
- [26] S. Monchocé, S. Kahaly, A. Leblanc, L. Videau, P. Combis, F. Réau, D. Garzella, P. D’Oliveira, P. Martin, and F. Quéré, Optically Controlled Solid-Density Transient Plasma Gratings, *Phys. Rev. Lett.* **112**, 145008 (2014).
- [27] A. Leblanc, A. Denoeud, L. Chopineau, G. Mennerat, P. Martin, and F. Quéré, Plasma holograms for ultrahigh-intensity optics, *Nat. Phys.* **13**, 440 (2017).
- [28] S. Schrauth, A. Colaitis, R. Luthi, R. Plummer, W. Hollingsworth, C. Carr, M. Norton, R. Wallace, A. Hamza, B. MacGowan, *et al.*, Study of self-diffraction from laser generated plasma gratings in the nanosecond regime, *Phys. Plasmas* **26**, 073108 (2019).
- [29] R. M. G. M. Trines, F. Fiúza, R. Bingham, R. A. Fonseca, L. O. Silva, R. A. Cairns, and P. A. Norreys, Production of Picosecond, Kilojoule, and Petawatt Laser Pulses via Raman Amplification of Nanosecond Pulses, *Phys. Rev. Lett.* **107**, 105002 (2011).
- [30] M. R. Edwards, K. Qu, J. M. Mikhailova, and N. J. Fisch, Beam cleaning of an incoherent laser via plasma Raman amplification, *Phys. Plasmas* **24**, 103110 (2017).
- [31] L. Lancia, J.-R. Marques, M. Nakatsutsumi, C. Riconda, S. Weber, S. Hüller, A. Mančić, P. Antici, V. Tikhonchuk, A. Héron, *et al.*, Experimental Evidence of Short Light Pulse Amplification Using Strong-Coupling Stimulated Brillouin Scattering in the Pump Depletion Regime, *Phys. Rev. Lett.* **104**, 025001 (2010).
- [32] G. Lehmann, F. Schluck, and K. H. Spatschek, Regions for Brillouin seed pulse growth in relativistic laser-plasma interaction, *Phys. Plasmas* **19**, 093120 (2012).
- [33] G. Mourou and T. Tajima, More intense, shorter pulses, *Science* **331**, 41 (2011).
- [34] N. M. Naumova, J. A. Nees, I. V. Sokolov, B. Hou, and G. A. Mourou, Relativistic Generation of Isolated Attosecond Pulses in a  $\lambda^3$  Focal Volume, *Phys. Rev. Lett.* **92**, 063902 (2004).
- [35] Z.-M. Sheng, J. Zhang, and D. Umstadter, Plasma density gratings induced by intersecting laser pulses in underdense plasmas, *Appl. Phys. B* **77**, 673 (2003).
- [36] S. H. Glenzer, *et al.*, Symmetric inertial confinement fusion implosions at ultra-high laser energies, *Science* **327**, 1228 (2010).
- [37] G. Lehmann and K. H. Spatschek, Transient Plasma Photonic Crystals for High-Power Lasers, *Phys. Rev. Lett.* **116**, 225002 (2016).
- [38] S. Suntsov, D. Abdollahpour, D. Papazoglou, and S. Tzortzakis, Femtosecond laser induced plasma diffraction gratings in air as photonic devices for high intensity laser applications, *Appl. Phys. Lett.* **94**, 251104 (2009).
- [39] L. Shi, W. Li, Y. Wang, X. Lu, and H. Zeng, Generation of High-Density Electrons Based on Plasma Grating Induced Bragg Diffraction in Air, *Phys. Rev. Lett.* **107**, 095004 (2011).
- [40] M. Durand, A. Jarnac, Y. Liu, B. Prade, A. Houard, V. Tikhonchuk, and A. Mysyrowicz, Dynamics of plasma gratings in atomic and molecular gases, *Phys. Rev. E* **86**, 036405 (2012).
- [41] I. Y. Dodin and N. J. Fisch, Storing, Retrieving, and Processing Optical Information by Raman Backscattering in Plasmas, *Phys. Rev. Lett.* **88**, 165001 (2002).
- [42] Y. Michine and H. Yoneda, Ultra high damage threshold optics for high power lasers, *Commun. Phys.* **3**, 1 (2020).
- [43] H. Peng, C. Riconda, M. Grech, J.-Q. Su, and S. Weber, Nonlinear dynamics of laser-generated ion-plasma gratings: A unified description, *Phys. Rev. E* **100**, 061201 (2019).
- [44] L. Friedland, G. Marcus, J. Wurtele, and P. Michel, Excitation and control of large amplitude standing ion acoustic waves, *Phys. Plasmas* **26**, 092109 (2019).
- [45] P. Zhang, N. Saleh, S. Chen, Z. Sheng, and D. Umstadter, Laser-Energy Transfer and Enhancement of Plasma Waves and Electron Beams by Interfering High-Intensity Laser Pulses, *Phys. Rev. Lett.* **91**, 225001 (2003).
- [46] P. Michel, L. Divol, E. A. Williams, S. Weber, C. A. Thomas, D. A. Callahan, S. W. Haan, J. D. Salmonson, S. Dixit, D. E. Hinkel, M. J. Edwards, B. J. MacGowan, J. D. Lindl, S. H. Glenzer, and L. J. Suter, Tuning the Implosion Symmetry of ICF Targets via Controlled Crossed-Beam Energy Transfer, *Phys. Rev. Lett.* **102**, 025004 (2009).
- [47] D. Turnbull, P. Michel, T. Chapman, E. Tubman, B. Pollock, C. Chen, C. Goyon, J. Ross, L. Divol, N. Woolsey, *et al.*, High Power Dynamic Polarization Control Using Plasma Photonics, *Phys. Rev. Lett.* **116**, 205001 (2016).
- [48] G. Lehmann and K. H. Spatschek, Plasma-based polarizer and waveplate at large laser intensity, *Phys. Rev. E* **97**, 063201 (2018).
- [49] X. Yang, J. Wu, Y. Tong, L. Ding, Z. Xu, and H. Zeng, Femtosecond laser pulse energy transfer induced by plasma grating due to filament interaction in air, *Appl. Phys. Lett.* **97**, 071108 (2010).

- [50] J. Liu, W. Li, H. Pan, and H. Zeng, Two-dimensional plasma grating by non-collinear femtosecond filament interaction in air, *Appl. Phys. Lett.* **99**, 151105 (2011).
- [51] M. Durand, Y. Liu, B. Forestier, A. Houard, and A. Mysyrowicz, Experimental observation of a traveling plasma grating formed by two crossing filaments in gases, *Appl. Phys. Lett.* **98**, 121110 (2011).
- [52] P. Yeh, *Introduction to Photorefractive Nonlinear Optics*, Wiley Series in Pure and Applied Optics (Wiley, 1993).
- [53] R. W. Boyd, *Nonlinear Optics, Inc.* (Academic Press, Orlando, FL, USA, 2008), 3rd ed.
- [54] T. D. Arber, K. Bennett, C. S. Brady, A. Lawrence-Douglas, M. G. Ramsay, N. J. Sircombe, P. Gillies, R. G. Evans, H. Schmitz, A. R. Bell, and C. P. Ridgers, Contemporary particle-in-cell approach to laser-plasma modelling, *Plasma Phys. Controlled Fusion* **57**, 113001 (2015).
- [55] M. R. Edwards, N. Fasano, N. Lemos, A. Singh, V. Munirov, E. Kur, J. Wurtele, J. Mikhailova, and P. Michel, in *CLEO: Fundamental Science* (Optical Society of America, San Jose, California, 2021).
- [56] N. Bonod and J. Neauport, Diffraction gratings: From principles to applications in high-intensity lasers, *Adv. Opt. Photonics* **8**, 156 (2016).
- [57] L. Rovige, J. Huijts, I. Andriyash, A. Vernier, V. Tomkus, V. Girdauskas, G. Raciukaitis, J. Dudutis, V. Stankevic, P. Gecys, *et al.*, Demonstration of stable long-term operation of a kilohertz laser-plasma accelerator, *Phys. Rev. ST Accel. Beams* **23**, 093401 (2020).
- [58] K. Schmid, A. Buck, C. M. Sears, J. M. Mikhailova, R. Tautz, D. Herrmann, M. Geissler, F. Krausz, and L. Veisz, Density-transition based electron injector for laser driven wakefield accelerators, *Phys. Rev. Accel. Beams* **13**, 091301 (2010).
- [59] S. Yoon, A. Goers, G. Hine, J. Magill, J. Elle, Y.-H. Chen, and H. Milchberg, Shock formation in supersonic cluster jets and its effect on axially modulated laser-produced plasma waveguides, *Opt. Express* **21**, 15878 (2013).
- [60] C. E. Clayton, J. Ralph, F. Albert, R. Fonseca, S. Glenzer, C. Joshi, W. Lu, K. Marsh, S. F. Martins, W. B. Mori, *et al.*, Self-Guided Laser Wakefield Acceleration Beyond 1 GeV Using Ionization-Induced Injection, *Phys. Rev. Lett.* **105**, 105003 (2010).
- [61] P. Poole, A. Krygier, G. Cochran, P. Foster, G. Scott, L. Wilson, J. Bailey, N. Bourgeois, C. Hernandez-Gomez, D. Neely, *et al.*, Experiment and simulation of novel liquid crystal plasma mirrors for high contrast, intense laser pulses, *Sci. Rep.* **6**, 32041 (2016).
- [62] M. R. Edwards, V. R. Munirov, A. Singh, N. Fasano, E. Kur, N. Lemos, J. M. Mikhailova, J. S. Wurtele, and P. Michel, Holographic Plasma Lenses, *Phys. Rev. Lett.* **128**, 065003 (2022).
- [63] G. Lehmann and K. Spatschek, Plasma volume holograms for focusing and mode conversion of ultraintense laser pulses, *Phys. Rev. E* **100**, 033205 (2019).
- [64] J. Palastro, D. Gordon, B. Hafizi, L. Johnson, J. Peñano, R. Hubbard, M. Helle, and D. Kaganovich, Plasma lenses for ultrashort multi-petawatt laser pulses, *Phys. Plasmas* **22**, 123101 (2015).
- [65] R. Wilson, M. King, R. Gray, D. Carroll, R. Dance, C. Armstrong, S. Hawkes, R. Clarke, D. Robertson, D. Neely, *et al.*, Ellipsoidal plasma mirror focusing of high power laser pulses to ultra-high intensities, *Phys. Plasmas* **23**, 033106 (2016).